Guardiola García, C.; Martín Díaz, J.; López Sánchez, JJ.; García Sarmiento, D. (2011). Semiempirical in-cylinder pressure based model for NOx prediction oriented to control applications. Applied Thermal Engineering. 31(16):3275-3286. doi:10.1016/j.applthermaleng.2011.05.048.

Semiempirical in-cylinder pressure based model for NO_X prediction oriented to control applications

C. Guardiola, J.J. López, J. Martín*, D. García-Sarmiento

CMT-Motores Térmicos, Universidad Politécnica de Valencia, Camino de Vera s/n, 46022, Valencia, Spain

Abstract

This work describes the development of a fast NO_X predictive model oriented to engine control in diesel engines. The in-cylinder pressure is the only instantaneous input signal required, along with several mean variables that are available in the ECU during normal engine operation.

The proposed model is based on the instantaneous evolution of the heat release rate and the adiabatic flame temperature (both obtained among other parameters from the in-cylinder pressure evolution). Corrections for considering the NO_X reduction due to the re-burning mechanism are also included. Finally, the model is used for providing a model-based correction of tabulated values for the NO_X emission at the reference conditions. The model exhibits a good behaviour when varying exhaust gas recirculation rate, boost pressure and intake temperature, while changes in the engine speed and injection settings are considered in the tabulated values.

Concerning the calculation time, the model is optimized by proposing simplified sub-models to calculate the heat release and the adiabatic flame temperature. The final result is suitable for real time applications since it takes less than a cycle to complete the NO_X prediction.

Keywords: NOx, heat release rate, adiabatic flame temperature, reburning

*Corresponding author. Tel: +34963877650; fax: +34963877659
Email address: jaimardi@mot.upv.es (J. Martín)
URL: www.cmt.upv.es (J. Martín)

April 19, 2011

Nomenclature

c_v	specific heat at constant volume	[J/kgK]
$\mathrm{d}Q_b$	heat release rate	[W]
ECU	engine control unit	
EGR	exhaust gas recirculation	[%]
EOC	end of combustion	[°]
FFT	fast Fourier transform	
F_r	fuel-air equivalence ratio	[-]
h	specific enthalpy	[J/kg]
IVC	intake valve closing	
K	constant	
m	mass	[kg]
n	engine speed	[rpm]
p	pressure	[bar]
Q	heat transfer to the walls and heat release	[J]
R	specific gas constant	[J/kg K]
SOC	start of combustion	[°]
SOI	start of injection	[°]
T	temperature	[K]
u	specific internal energy	[J/kg]
V	volume	[m^3]
Y	mass fraction	[-]

Subscripts

0	reference operating conditions
a	air
ad	adiabatic
b	stoichiometric combustion products
$base$	base model
bb	*blow-by*
c	gas mean properties in the chamber
$comb$	current combustion
cyl	in-cylinder
$diss$	dissociation
exh	exhaust manifold
exp	experimental measurements
f	fuel
f, ev	fuel evaporation
f, g	gaseous fuel
f, inj	liquid fuel at injection conditions
inj	injection
itk	intake manifold
IVC	intake valve closing
$main$	main injection
net	net production at current cycle
nd	non-dissociated species
NO_X	nitrogen oxides
O_2	oxygen
pil	pilot injection
re	re-burning
ub	unburned gas

Greek symbols

α	crank angle
γ	adiabatic coefficient
ϵ	NO_X reduction efficiency

1. Introduction

The compression ignition engine is today the most efficient engine for transport applications in terms of fuel consumption; nevertheless its pollutant emissions still represent a major environmental challenge. For the implementation of active control methods, and also the control of after-treatment systems, a proper modelling of the pollutants production can be a reliable alternative to the gas composition sensors that are being developed[1, 2]. One of the main pollutants in compression ignition engines are nitrogen

oxides (NO_X). NO_X are produced during basically all kinds of combustions and their formation can be divided into four different types: thermal NO_X formation, fuel NO_X formation, prompt NO_X formation and finally via N_2O. As it will be justified, this work is focused only on the thermal NO_X production.

Several models that predict the amount of NO_X emission released by diesel engines have been published [3–6]. Some of them are based on correlations of the NO_X production with different operation variables[7], while others account for the in-cycle evolution of the NO_X. Between these last, some of them use the in-cylinder pressure signal as an input quantity[3, 8, 9]. The in-cylinder pressure is considered a valuable signal because it provides direct information of the combustion development, as for example the peak pressure or the indicated mean effective pressure. Moreover, in-cylinder pressure can allow some more complex engine control applications such as air mass flow estimation [10], on-line combustion detection [11] or failure detection [12], exhaust gas recirculation control [13], torque estimation [14] or noise control [15]. In this work, in-cylinder pressure will be used as a basic input signal for predicting the NO_X emission for control oriented applications, on the basis of the calculation of the heat release and the adiabatic flame temperature during the combustion process.

Although this kind of models that track the instantaneous NO_X production suppose a non negligible computational burden, recent evolution in the control unit computational power makes it possible apply them for the engine control and diagnosis. In that sense [8, 9, 16] have proposed models that integrate reliable NO_X estimations with almost real time calculations. The use of these fast predictive models combined with closed-loop control of the injection settings and air loop control settings has a big potential on novel technologies oriented for both diminishing NO_X production during combustion as well as improving deNO_X aftertreatment. As an example, there are some works [17, 18] in which NO_X prediction models allows to optimise the control of the reduction agent flow into the catalytic converter, using only the minimum necessary amount and thus extending its lifetime.

A key issue when dealing with NO_X prediction models oriented to control applications is to maintain a good equilibrium between accuracy and calculation time. Regarding this point two extreme options can be considered: physical modelling approach, or experimental mapping of the NO_X emitted by a reference engine as a function of engine speed and load. The first option provides a physical representation of the problem, providing prediction capabilities when the engine is in off-design operation, while the second option has clear computational advantages, and also can be more precise as far as the engine operation is close to the nominal situation.

The model proposed in this work combines a fast physical-based model and a set of empirical look-up tables with the reference values for the nominal conditions. Tabulated values are used for providing a nominal value of the NO_X production, while heat release profile and the adiabatic flame temperature are calculated from in-cylinder pressure and their evolution is then compared with the nominal situation to provide a NO_X correction to be applied. Additionally, the proposed model does not only considers the NO_X formation, but its reduction when NO_X molecules are re-entrained in the spray (known in the literature as re-burning[1]).

The paper is structured as follows: section 2 provides a description of the engine and the experimental set-up used to obtain the data for the model development. Section 3, 4 and 5 are devoted to the description of the base NO_X model, the correction due to the

reburning process and the approach used for the online calculation respectively. Finally sections 6, 7 and 8 present the model validation and discussion, some computational issues and the main conclusions.

2. Experimental Setup

A schema of the test cell layout with the instrumentation is shown in Figure 1. The experimental tests presented in this work were carried out in a high speed direct injection diesel engine with 2.2-litre of total displacement that is currently in production. It is a four-cylinder engine with sequential parallel turbo-charger[19] equipped with a Bosch common rail injection system. The engine main characteristics are given in Table 1.

The in-cylinder pressure was measured in one of the cylinders by means of a Kistler 6055B glow-plug piezoelectric transducer, with a range between 0 and 250 bar and a sensitivity of 18.8 pC/bar. The pressure sensor was calibrated according to the traditional method proposed in [20]. Angle-synchronous acquisition was used for the in-cylinder pressure. For this purpose an optical encoder providing two signals was used: the first is a pulse at each crankshaft revolution, which is used as trigger signal; the second is an external clock for the instantaneous acquisition system with a 0.5° sampling interval.The trigger, the external clock and the in-cylinder pressure signals are fed to the acquisition system, a Yokogawa DL708E oscillographic recorder. Several mean variables (acquired at a constant sample frequency of 100 Hz) are necessary for controlling the engine operating point and also for the model calculation; an AVL tests system is used for this purpose. The values of the inlet pressure and temperature and fresh admitted air were also collected from the ECU. The exhaust emissions were analysed and recorded using an exhaust monitoring equipment (Horiba MEXA 7100 D), and the intake manifold CO_2 concentration was also measured for determining the EGR rate.

The comparison between the mean values obtained from the AVL tests system and the engine ECU showed a mean relative error of about 2%. Such difference was considered small enough to use directly the ECU values, which is coherent with the aim of the model, that is, to be used in control applications.

For the definition of the test matrix the variables affecting NO_X and the foreseen application of the model were considered. According to [21, 22], the parameters affecting NO_X formation can be grouped into two possible sources: the intake conditions (T_{itk}, p_{itk} and gas composition depending on the EGR rate) and fuel injection parameters (injection pressure -p_{inj}-, injection strategies: start of main injection -SOI$_{main}$- and pilot injection -SOI$_{pil}$-). Molina [22] performed a sensitivity study of p_{inj} and SOI$_{main}$, evaluating their influence over NO_X emissions. He concluded that p_{inj} is more effective than SOI$_{main}$, since for the same NO_X reduction (respect to the nominal value) the penalty in fuel consumption is smaller than modifying the injection timing (SOI$_{main}$ must allow a centred combustion in order to maximise the engine performance, and SOI$_{pil}$ is optimized according to combustion noise restrictions). If a parametric variation of the injection parameter is considered, this conclusion would allow to rank those parameters according of their influence.

Nevertheless, the model is intended to be used for the control of current diesel engines, where injection settings are programmed as a function of engine load and speed. Hence the experimental plan will be based on the assumption that the injection settings are fixed, while parametric studies are run for EGR rate, intake pressure p_{itk} and intake

temperature T_{itk}. Such variations are similar to those occurring during load and speed transients during realistic engine operation.

Figure 2 summarises the variation ranges for the experimental tests; the data set has been divided into a training data set and a validation data set. The experimental plan included 14 reference operating points at different speeds and loads for the model development and 24 for its validation, as shown in Table 2. At each operating point variations of the EGR rate (from 0% to 58% EGR at low load and up to 25% at high load), the boost pressure (up to 1 bar variation with regard to the nominal operation) and inlet temperature (up to 40 K variation) were performed.

3. Base NO_X model

In this section the basic NO_X model is presented. This model will be reformulated in section 5 in order to be used as a corrective factor based on the measured in-cylinder pressure. The basic model is based on the one presented by Arrègle *et al.* [9] which, in order to increase its reliability and accuracy, has been modified with an improved heat release calculation (which will be presented in section 3.1) and the inclusion of a NO_X emission correction based on re-burning mechanism (shown in section 4).

Although the basic model is based on the NO formation, rather than the NO_X, in this work we will refer generically to NO_X because NO formation and NO_X emission are assumed to be correlated, and because the final model will be adjusted to fit experimental tailpipe NO_X emissions. Hence, no specific distinction will be made between both quantities.

The basic model in [9] is based on the Zeldovich thermal NO_X mechanism [23, 24]. The NO_X formation is exponentially dependent on temperature, and thus the local areas with higher temperature than the average can have a very large impact on the quantity of NO_X produced. However a complete tracking of the NO_X kinetic is discarded because two reasons:

- It seems incompatible with the ECU computation capability; this could be solved using a parametrisation of the Zeldovich mechanism, reducing the computation requirements [25].
- A complete tracking makes no sense without a proper description of the flame. This second issue is out of the scope of a control oriented model.

The simplified approach uses the adiabatic flame temperature (T_{ad}) profile, since it is assumed that NO_X production is related to the combustion chamber maximum local temperature [26], and the heat release profile ($\mathrm{d}Q_b$), since assuming that the fuel is burned with a given relative fuel-air equivalence ratio ($F_r = 1$) for the combustion products formation, and thus NO_X production, is correlated with the instantaneous heat release rate. From these hypotheses, the base NO_X model according to [9] is:

$$m_{NO_x,base} = \int_{\alpha} \mathrm{d}Q_b(\alpha) \cdot K_1 \cdot \left(\frac{n}{2000}\right)^{K_2} \cdot e^{\left(\frac{K_3}{T_{ad}(\alpha)}\right)} \mathrm{d}\alpha \tag{1}$$

where $\mathrm{m}_{NO_X,base}$ is the total predicted NO_X mass per cycle, n is the engine speed and K_1, K_2 and K_3 are constants. According to [27] the term including the engine speed

is due to the fact that at higher engine speeds fuel is consumed in a much shorter time period by the enhanced fuel/air mixing process, shortening the combustion duration providing less available time for NO_X formation.

3.1. Heat release rate calculation

The heat release rate is the rate at which the chemical energy of the fuel is released by the combustion process and, as stated in equation (1) dQ_b is proportional to NO_X formation. dQ_b can be calculated from in-cylinder pressure versus crank angle data, with different levels of complexity and accuracy [28, 29]. In the previous work [9] the heat release was calculated with a fast heat release expression based on the first law of thermodynamics. This kind of calculation is very suitable for the ECU capabilities but it has an important effect on the accuracy of the predictions, as it will be shown later. Thus, for the sake of precision, a more complex and hence slightly slower, calculation is proposed, which is an evolution of the one presented in [30].

The main input of the combustion diagnosis model (i.e. code for calculating the heat release) is the in-cylinder pressure and some mean variables available in the ECU: air and fuel mass flows, temperature and pressure in the manifolds, coolant temperature, engine speed and injection settings (start and duration of each pulse).

The diagnosis model solves the first law and the gas equation of state between intake valve closing (IVC) and exhaust valve opening to obtain the rate of heat released and the instantaneous mean temperature in the chamber. For such calculation, the model considers that the pressure is uniform in the combustion chamber and the gas is assumed to be a perfect mixture of three perfect gases (air, gaseous fuel and stoichiometric burnt products). Gas properties are calculated through correlations considering the mean chamber temperature. The model also accounts for convective heat transfer to the walls [31, 32], and blow-by leakage.

The final expression of the first law obtained is:

$$\mathrm{d}Q_b = m_c c_{v,c} \mathrm{d}T + \mathrm{d}Q + p\mathrm{d}V - (h_{f,inj} - u_{f,g}) \cdot \mathrm{d}m_{f,ev} + R_c T_c \mathrm{d}m_{bb} \qquad (2)$$

where m_c is the mass of the mixture contained in the combustion chamber, $c_{v,c}$ is the specific heat at constant volume of the mixture, Q is the heat transferred to the walls, p and V are the in-cylinder pressure and volume, $h_{f,inj}$ stands for the injected fuel specific enthalpy and $u_{f,g}$ for the gaseous fuel energy of the evaporated fuel mass $m_{f,ev}$. The last term in the expression accounts for the blow-by leakage m_{bb}, characterised by the combustion chamber specific gas constant R_c and mean temperature T_c.

In order to solve equation (2) several sub-models are combined [33]. Figure 3 illustrates the calculation sequence of the different sub-models.

The initial simplified model for dQ_b calculation as used in [9] took about 2 ms per engine cycle in a 3 GHz PC, while the detailed calculation using the code presented in [30] consumed 484 ms, which was far away of a real-time application scenario. In order to overcome this problem, some of the sub-models with high computational cost were simplified or optimised. The main actions consisted on the elimination of some non-critical calculation sub-models (such as fuel evaporation), the substitution of slow sub-models (such as the filling-emptying model used to estimate the trapped mass) by others simpler and faster [34] and the simplification of the pressure processing (pressure pegging using the intake pressure instead of a thermodynamic criterion and fast filtering

instead of FFT). With such strategies, the final time for calculating the dQ_b was about 2.5 ms, near to the time consumed by the initial simplified model but providing a higher accuracy. The benefits of this improved accuracy will be demonstrated in section 5.

3.2. Calculation of the adiabatic flame temperature

The temperature in a combustion process in the absence of heat losses to the surroundings is commonly referred to as the adiabatic flame temperature, which corresponds to the maximum temperature that can be achieved for some given reactants, because any heat transfer or work from the reacting substances and any incomplete combustion would tend to lower the temperature of the products.

Figure 4 shows an schema of the procedure for calculating T_{ad} taking into account dissociation effects. From the known value of the air mass fraction at IVC, $Y_{a,IVC}$, the oxygen mass fraction $Y_{O_2,IVC}$ can be directly derived. In addition to the gas composition, the other key variable for the adiabatic flame temperature calculation is the unburned gas temperature (T_{ub}), which can be calculated assuming that the heat losses to the walls of the combustion chamber from the unburned gas and the heat transfer from the flame are equal. The unburned gas temperature at the start of combustion (SOC) is obtained from the thermodynamic diagnosis model. From this value, the instantaneous T_{ub} is calculated with the expression of an isentropic compression:

$$T_{ub} = T_{ub-1} \cdot \left(\frac{p_{cyl}}{p_{cyl-1}} \right)^{\left(\frac{\gamma-1}{\gamma}\right)} \tag{3}$$

where p_{cyl}, T_{ub}, p_{cyl-1} and T_{ub-1} are the in-cylinder pressure and temperatures at the current angle and at the previous angle respectively.

Once $Y_{O_2,IVC}$ and T_{ub} evolution along the cycle are calculated, the following expression is used for determining the adiabatic flame temperature during the diffusion combustion process [9]:

$$T_{ad}(\alpha) = T_{ub} + \Delta T_{nd}\,(\alpha) - \Delta T_{diss}\,(\alpha)\,; \quad \Delta T_{nd} = 37630.5 \cdot \left(\frac{Y_{O_2}}{3.48 \cdot F_r} \right) \tag{4}$$

$$\text{If} \quad T_{ub} + \Delta T_{nd}\,(\alpha) < 2600K; \quad \Delta T_{diss}(\alpha) = 1.554 \cdot 10^{-7} \cdot \left(T_{ub} + \Delta T_{nd}\right)^{2.677}(\alpha) \tag{5}$$

$$\text{If} \quad T_{ub} + \Delta T_{nd}\,(\alpha) > 2600K; \quad \Delta T_{diss}\,(\alpha) = 7.136 \cdot 10^{-10} \cdot \left(T_{ub} + \Delta T_{nd}\right)^{3.36}(\alpha) \tag{6}$$

where the combustion temperature is the result of the unburnt gas temperature T_{ub}, the shift in the temperature due to the heat released during the combustion ΔT_{nd}, and a correction ΔT_{diss} according to the expressions (5) and (6), that accounts for the energy absorbed by the partial dissociation of the combustion products CO_2, H_2O, N_2 and O_2 into CO, H_2, H, OH, O, NO and N (see [9] for further details).

As an illustrative example, Figure 5 shows the calculated evolution of the different temperatures (unburnt gas temperature, flame temperature without considering species dissociation and the final calculation the adiabatic flame temperature) for one of the experimental test at 2500 rpm and 58% load. It must be highlighted that all the involved mechanisms are significant and may not be neglected.

3.3. Fitting of the base NO_X model constants

The fitting process consists on determining the values for K_1, K_2 and K_3 in expression (1). First step in this process is deciding if the general constant values will be fitted for the whole operating range of the engine, or if a local optimisation will be used and then the different constants are programmed as a function of a set of operating parameters (as engine speed or load). Local fitting of the model can be also used for determining the suitability of using the global approach. For that, an individual set of constants $\{K_1, K_2, K_3\}$ is obtained for each nominal condition (considering the nominal test and the parametric study performed for that engine speed and load).

Note that as engine speed is kept constant when varying EGR rate, boost pressure and intake manifold temperature, it is not possible to provide an estimate for K_1 and K_2 independently but $K_1 \left(n/2000\right)^{K_2}$ must be fitted as a group.

Figure 6 shows the values of the constants obtained in each operating condition tested according to Table 2, for both training and validation operating points. Each point in Figure 6 corresponds to the optimal selection of the model constants for minimising the error of the group of tests obtained varying p_{itk}, T_{itk} and EGR rate at a given engine speed and load. As it can be appreciated K_3 exhibits a quite constant value, while $K_1 \left(n/2000\right)^{K_2}$ strongly depends on the operating conditions. The first row in Table 3 shows the mean average error of the local fit of the model for all the tests in the experimental plan.

On the other hand, global constants can be fitted using a global approach. For that, a least squares algorithm was used to obtain global values for $\{K_1, K_2, K_3\}$, using only the data set corresponding to the training tests in Table 2. Then, these constants were used for the whole operating range of the engine, for both training and validation operating points. Figure 6 depicts the evolution of the fitted $K_1 \left(n/2000\right)^{K_2}$ and K_3, and its comparison with the local values. Mean estimate errors for the training and validation data set are shown in the second row of Table 3.

Note that, according to Table 3, the local fit always provides more precise results than the global fit of the model, which is straightforwardly derived from the fitting concept. However, as the variation of K_3 along the operation range of the engine is limited (the variation coefficient is 0.7%), it is possible to consider a global K_3 while using a local fit of the two other model coefficients. Such approach will be considered in section 5. It is also interesting to highlight that the mean absolute errors obtained with the validation data are higher than those obtained using the training data. This is because the model was trained with operating conditions ranging from idle to 3000 rpm at partial loads, where the NO_X produced are low (less than 2 mg/str) in comparison to the whole engine map (up to 8.5 mg/str at full load and high speed) that was used for the validation. This issue will be discussed in section 6.

Figure 7 shows an example of the predicted vs. experimental NO_X emissions obtained in a parametric variation of EGR rate, boost pressure and intake temperature, after the described local fit approach. Two operating points at 2000 rpm are represented, one at very low load (15%) and the other at medium-high load (58%). As can be seen the model is able to correctly predict the trends in the NO_X when a variation in any of the three parameters is performed. The observed trends can be easily justified:

- EGR variation: according to Ladommatos *et al.* [21], when the exhaust gases

are recirculated the displacement of inlet charge with CO_2 and H_2O affects the combustion process through three main effects: dilution, thermal and chemical effect. The greater reduction of NO_X emissions is reached by the thermal effect, and it is mainly because when the Y_{O_2} goes down in the combustion chamber, the T_{ad} decreases too, directly influencing the NO_X production.

- T_{itk} variation: the intake temperature was progressively raised from 336 to 360K, keeping p_{itk} constant. This parameter increases the NO_X level due to two effects. First a variation of T_{itk} directly affects T_{ad} through T_{ub} (as explained in section 3.2), the second is a reduction of the ignition delay and, thus the combustion is advanced, raising the gas temperature T_{ub}.

- p_{itk} variation: in agreement with the equation of state, when the pressure is increased (maintaining T_{itk} constant), the density also increases thus improving the air-fuel mixture thus accelerating the combustion and also increasing the gas temperature T_{ub}. Additionally when the boost pressure increases (keeping the inlet temperature and the EGR rate) the fresh air mass flow increases and therefore air-fuel ratio gets lower, thus increasing the oxygen composition and T_{ad}. As a result of these variations, NO_X emissions increases significantly.

According to Figure 7 it can be stated that the model behaves better when EGR variations re introduced, since it has the lowest error. This trend is also followed at different operating points, with a mean relative error of 13.2% in the EGR variations versus 18.4% in the p_{itk} and 21.3% in the T_{itk} parametric studies. This can be attributed to the model sensitivity to changes in T_{ad} which is directly related to $Y_{O_2,IVC}$. The influence of the EGR rate over T_{ad} is a combination of several effects, besides the mentioned main effect on $Y_{O_2,IVC}$. According to Molina [22], the EGR rate affects the adiabatic coefficient γ decreasing its value [35], which is a term of equation (3) used for the calculation of T_{ub}; both effects are reflected on equation (4).

4. Model correction based on NO_X reduction mechanism

Although most of the predictive NO_X models only take into account the NO_X formation mechanism, if the NO_X reduction mechanism in the flame is considered the accuracy of the basic model presented in the previous section can be improved. According to the diesel diffusion flame model proposed by Dec [36], the local conditions inside of a quasi-steady diffusion flame (a region with high temperatures not far from the adiabatic flame temperature, and a mixture of both burned and cracked fuel gases) correspond to an even more reducing atmosphere than that in the re-burning zone of a thermal power plant, where an important NO_X reduction rate is achieved [37, 38]. Taking into account this effect, a NO_X reduction model is proposed. The model considers that the NO_X going through the reacting spray cone from two possible sources:

1. From exhaust gases in the combustion chamber coming from internal (residual gases) or external EGR.
2. The NO_X produced in the current combustion that can be re-entrained into the reduction zone of the flame.

When the NO_X molecules are entrained in the spray, the model considers that they go through the reductive atmosphere existing inside the diffusion flame and part of them are reduced thus disappearing [39]. The percentage of disappearance depends on the local temperature and composition as well as on the residence time, and it is strongly linked to the mixing rate of the combustion products [40].

The complete formation and reduction process is represented in Figure 8. Appendix A provides details of NO_X reduction mechanism formulation that allows to derive the following equation:

$$Y_{NO_X,exh} = \frac{m_{NO_X,comb} \cdot (1 - K_{re} \cdot Fr \cdot \varepsilon)}{m_a + m_f + m_{EGR} \cdot Fr \cdot \varepsilon} \tag{7}$$

where $Y_{NO_X,exh}$ stands for the NO_X mass fraction at the exhaust, $m_{NO_X,comb}$ is the NO_X mass produced at the current combustion, m_a, m_f and m_{EGR} are the fresh air, fuel and EGR mass respectively, Fr is the fuel-air equivalence ratio, K_{re} is the fraction of gas re-entrained (0.5 used here, see Appendix A), and ε is the efficiency of the NO_X reduction (1 used here, see Appendix A).

Taking into account the effect of the NO_X reduction mechanism, the net NO_X emitted in each cycle can be expressed as follows:

$$m_{NO_X,re} = Y_{NO_X,exh} \cdot (m_a + m_f) \tag{8}$$

where $m_{NO_X,re}$ is the net NO_X emitted considering reburning, and $Y_{NO_X,exh}$ is calculated with equation (8), where it is assumed that $m_{NO_X,comb}$=$m_{NO_X,base}$, calculated with equation (1).

The constants K_1, K_2 and K_3 (used for the $Y_{NO_X,exh}$ calculation) were fitted again using the training operating points used for the base model in section 3.3. Figure 9 shows the measured and predicted values before and after the re-burning correction (top), and the corresponding relative error when varying EGR rate (from 0% to 32%) at 2500 rpm and 45% load. As it can be noticed, the prediction error is slightly reduced for all the cases. In the rest of operating points (not shown) this trend is also followed. Compared with the results obtained in section 3.3, the mean relative error of the global study is improved about 1.3% by the NO_X reduction mechanism correction.

5. Empirical correction

According to section 3.3 the model coefficient K_3 is quite constant, while important variations are obtained in the two other model coefficients. As an intermediate step between the local and global approach for the model fitting, tabulated values for $K_1\,(n/2000)^{K_2}$ while a global value for K_3 will now be used. This is a way of profiting the high repeatability found in constant K_3 of the model while keeping the flexibility of the local fitting approach for adapting to different operating conditions. Next it will be proved that using local K_1 and K_2 is equivalent of normalising the NO_X production with a nominal operating condition:

$$m_{NO_X} = m_{NO_{X,0}} \frac{m_{NO_X,re}}{m_{NO_X,re,0}} \tag{9}$$

where $m_{NO_{X,0}}$ is the NO_X production at the reference operating conditions, and $m_{NO_X,re}$ is the prediction delivered by the model described in the previous section (which depends on the actual measurements, including the in-cylinder pressure). $m_{NO_X,re,0}$ stands for the model prediction at the nominal conditions (which can be calculated beforehand).

For the present work nominal conditions are selected as those with nominal settings (according to ECU calibration) at the considered engine speed and load. According to the usual control algorithms, that means that the reference situation has the same injection settings (number and disposition of injections, rail pressure control reference) than the actual operating point, and the model only has to compensate the deviations in the air loop or working temperature, what is consistent with the assumptions made on the experimental plan in section 2.

Combining expression (9) with the model according to equation (1), (7) and (8), and considering that the terms depending on K_1 and K_2 in equation (1) are cancelled because both the reference point and the considered conditions share the same engine speed and constants, equation (9) can be written as:

$$m_{NO_X} = m_{NO_X,0} \cdot \frac{(A \cdot B_0)}{(A_0 \cdot B)} \tag{10}$$

with:

$$\mathrm{A} = \left(\int_{\alpha} \mathrm{d}Q_b\left(\alpha\right) \cdot e^{\left(\frac{K_3}{T_{ad}(\alpha)}\right)} \mathrm{d}\alpha \right) \cdot \left(1 - K_{re} \cdot \left(\frac{m_a}{m_f}\right) \cdot \varepsilon\right) \cdot \left(m_a + m_f\right)$$

being the NO_X mass predicted by the model at the current operating conditions, and A_0 the equivalent term at the nominal conditions. And

$$B = m_a + m_f + m_{EGR} \cdot \left(\frac{m_f}{m_a}\right) \cdot \varepsilon$$

is a mass term affected by the reduction constant ε at the considered operating conditions, and B_0 at the reference conditions. Note that the ratio $m_{NO_X,0} \cdot B_0/A_0$ can be precomputed and stored according to a look-up table approach. Hence in the final model only A (derived from T_{ad} and $\mathrm{d}Q_b$ evolutions) and B (derived from mean variables obtained form the ECU) are calculated and used for correcting the tabulated value.

Note that equation (10) implies to assume that the model proposed in the previous section is able to correctly predict the variations with respect to the reference point when the EGR rate, p_{itk} or T_{itk} are changed, but it cancels any bias error in the reference point because the model, according to expression (9), would result in m_{NO_X,exp_0} for the reference conditions. This fact is demonstrated in Figure 10, where the original model and the one using the reference condition are compared. The later property can be also used for engine diagnosis: the deviation of the predicted NO_X value, with respect to the experimental value at the reference operating point, is an estimation of the degradation of the engine (e.g. when it is new and after several thousands of hours of operation).

Besides the accuracy improvement, it is interesting to note that the empirical correction leads to have only one model constant K_3, thus acquiring a higher robustness. Note that according to Figure 6 only the estimate of K_3 was shown to be consistent along the whole engine operation range. A value of $K_3 = -48767$ was fitted using the training operating points used for the previous model fittings (which slightly differs from the value shown in Figure 6 because now the re-burning correction is considered). Figure 11 shows an scatter plot of the prediction obtained for all the data set, including both training and validation sets; error metrics are summarised in Table 3 which are consistently better

than those exhibited by the global fitting approach.

6. Model validation

As stated, the model was fitted exclusively using the training data set that was constructed according to the second column of Table 2. This tests matrix corresponds to partial load tests at several engine speeds. It is important to emphasise that the engine speed for the model fitting only reaches up to 3000 rpm; this was done because the main objective for the model development was the EGR zone, restricted to engine speeds below 3100 rpm. However, the validation data set covers the complete engine map, including operating points at 3500 and 4000 rpm in a wide range of loads, even full load tests. Hence the validation covers significant extrapolations of the engine operating range (although the bias is corrected thanks to the empirical correction).

The complete matrix is detailed in the third column of Table 2 and characteristics of the applied variations in EGR, p_{itk} and T_{itk} are shown in Figure 2. At operating points in which there is no EGR in the original settings, no EGR variation was performed, but p_{itk} and T_{itk} variations were tested. In all cases, the reference conditions for the final model were those of the original ECU calibration.

The grey points in Figure 11 correspond to the measured and predicted NO_X values for the validation data set, including all variations in EGR, p_{itk} and T_{itk}. As can be seen, the model keeps its linear trend in the complete range of tests. The prediction errors are summarised in last row of Table 3, which do not importantly differ of those obtained in the model fitting. Although the model has been extrapolated (validation tests are out of the training data set range), the use of an empirical correction based on the measured NO_x at the reference conditions made possible to avoid great errors.

7. Computational issues

As previously stated, an important issue for control applications is the calculation time. The simplified combustion diagnostic code that feeds the model takes 2.5 ms to calculate dQ_b using a crank-angle step of 0.2°. With the algorithm proposed in section 3.2, T_{ad} can be calculated in 1.1 ms plus. The calculation time of the NO_X model is 0.9 ms in a 3 GHz PC using a Matlab code, thus the total calculation time of the final model is about 4.5 ms. Table 4 summarises the total calculation times and errors (for the parametric study varying EGR rate) using the 3 methods stated in section 3.1 for the heat release estimate: the original model [9] with fast heat release calculation and no corrections (method 1), the complete diagnosis code with all the submodels proposed in [30] (method 2) and the optimized heat release calculation with the corrections (method 3). The data acquisition time, about 4.5 ms plus, has not been included in the total calculation time in any case.

Considering the results obtained with the different methods, it can be concluded that the proposed model is slightly slower than the fast method but it increases importantly the final accuracy. In any case, as the total calculation time is smaller than an engine cycle, method 3 is considered fast enough for being computed on a real-time approach and to handle with transients test. In comparison with similar NO_X models [3, 8, 16] the proposal is faster (1 s, 0.5 s and 0.1 s respectively), probably because these other

models are not optimised in this aspect, as Hountalas *et al.* [16] recognises in their work. Moreover, the calculation time of these models is comparable to that of method 2 where the heat release calculation algorithm was the starting point for the optimised heat release calculation. Regarding the accuracy, the proposed model has a global mean error of about 15%, lower than the 23% of Egnell *et al.* proposal [3] and in the order of the one of Andersson *et al.* [8], although the direct comparison is difficult because they are considering different engines and operating conditions.

8. Conclusions

A control oriented model for raw NO_x emission has been presented. The main model inputs are the in-cylinder pressure evolution and other operative variables that are commonly available in any automotive ECU (air mass flow, injected, fuel mass, etc.). The in-cylinder pressure signal is used for tracking the NO_X formation through the thermal mechanism, on the basis of the flame temperature estimation. NO_X reduction through the re-burning process is also considered. Finally, the model is used for providing a local correction to the tabulated NO_X produced at a given engine load and speed.

The model has proved its capability to properly predict the effect of variations in the intake mix composition (EGR rate), boost pressure and intake temperature, on the NO_X production; the extrapolation of the model beyond its fitting range has proven its robustness.

Concerning the calculation time, it was optimized by proposing simplified sub-models to calculate dQ_b and T_{ad} in about 3.5 ms per engine cycle, plus 1 ms to compute the NO_X emissions. This calculation time is suitable for real time applications.

References

[1] J. Arregle, J.J. López, C. Guardiola and C. Monin, On board NOx prediction in diesel engines: A physical approach, in *Automotive Model Predictive Control: Models, Methods and Applications (Lecture Notes in Control and Information Sciences)*, Berlin:Springer (2010).

[2] R. Moos, A brief overview on automotive exhaust gas sensors based on electroceramics, Int. J. Appl. Ceram. Technol. 2 (2005) 401–413.

[3] R. Egnell, Combustion Diagnostics by Means of Multizone Heat Release Analysis and NO Calculation, SAE Paper 981424 (1998).

[4] D.J. Timoney, J.M. Desantes, L. Hernández and C.M. Lyons, The development of a semi-empirical model for rapid NO_X concentration evaluation using measured in-cylinder pressure in diesel engines, Proc. Inst. Mech. Eng. Part D-J. Automob. Eng. 219 (2005) 621–631.

[5] D. Cipolat, Analysis of energy release and NO_X emissions of a CI engine fuelled on diesel and DME, Appl. Therm. Eng. 27 (2007) 2095–2103.

[6] J.J Hernández, J. Pérez-Collado and J. Sanz-Argent, Role of the Chemical Kinetics on Modeling NO_X Emission in diesel Engines. Energy & Fuels 22 (2008) 262-272.

[7] M. Hirsch, K. Oppenauer, and L. del Re, Dynamic engine emission models, in *Automotive Model Predictive Control: Models, Methods and Applications (Lecture Notes in Control and Information Sciences)*, Berlin:Springer (2010).

[8] M. Andersson, B. Johansson, A. Hultqvist and C. Noehre, A Predictive Real Time NO_X Model for Conventional and Partially Premixed diesel Combustion, SAE Paper 2006-01-3329 (2006).

[9] J.Arregle, J.J. López, C. Guardiola and C. Monin, Sensitivity Study of a NO_X Estimation model for On-Board Applications, SAE Paper 2008-01-0640 (2008).

[10] J.M. Desantes, J. Galindo, C. Guardiola, V. Dolz, Air mass flow estimation in turbocharged diesel engines from in-cylinder pressure measurement, Exp. Therm. Fluid Sci. 34 (2010) 37–47.

[11] J.M. Luján, V. Bermúdez, C. Guardiola, A. Abbad, A methodology for combustion detection in diesel engine through in-cylinder pressure derivative signal, Mech. Syst. Signal Pr. (2010), doi:10.1016/j.ymssp.2009.12.012.

[12] S. Leonhardt, N. Müller, R. Isermann, Methods for engine supervision and control based on cylinder pressure information, IEEE/ASME Transactions on mechatronic 4 (1999) 235–245.

[13] M. Hasegawa, Y. Shimasaki, S. Yamaguchi, M. Kobayashi, M. Sakamoto, N. Kitayama, T. Kanda, Study on ignition timing control for diesel engines using in-cylinder pressure sensor, SAE paper 2006-01-0180 (2006).

[14] Y. Shimasaki, M. Kobayashi, H. Sakamoto, M. Ueno, M. Hasegawa, S. Yamaguchi, T. Suzuki, Study on engine management system using chamber pressure sensor integrated with spark plug, SAE Paper 2004-01-0519 (2004).

[15] F. Payri, A. Broatch, B. Tormos, V. Marant, New methodology for in-cylinder pressure analysis in direct injection diesel engines - application to combustion noise, Meas. Sci. Technol. 16 (2005) 540-547.

[16] D.T. Hountalas, N. Savva and R.G. Papagiannakis, Development of a New Physically Based Semi-empirical NO_X Model Using the measured Cylinder Pressure, THIESEL 2010 Conference on Thermo- and Fluid Dynamic Processes in Diesel Engines (2010).

[17] M. Devarakonda, G. Parker, J.H. Johnson and V. Strots, Model-based control system design in a urea-SCR aftertreatment system based on NH_3 sensor feedback, Int. J. Automot. Technol. 10 (2009) 653–662.

[18] S.R. Katare, J. E. Patterson and P. M. Laing, Diesel Aftertreatment Modeling: A Systems Approach to NO_X Control, Ind. Eng. Chem. Res 46 (2007) 2445-2454.

[19] J. Galindo, H. Climent, C. Guardiola, A. Tiseira and J. Portalier, Assessment of a sequentially turbocharged diesel engine on real-life driving cycles, Int. J. Vehicle Design 49 (2009) 214–234.

[20] J. Tichy, G. Gautschi, Piezoelektrische Messtechnik, Springer Verlag, Berlin, 1980.

[21] N. Ladommatos, S. Abdelhalim and H. Zhao, Control of oxides of nitrogen from diesel engines using diluents while minimising the impact on particulate pollutants, Appl. Therm. Eng. 18 (1998) 963–980.

[22] S. Molina, Influencia de los parámetros de inyección y la recirculación de gases de escape sobre el proceso de combustión en un motor diesel, Editorial Reverté,Barcelona, 2005.

[23] Y.A Zeldovich, The Oxidation of Nitrogen in Combustion and Explosions, Acta Physicochim. USSR 21 (1946) 577–628.

[24] C.P. Fenimore, Formation of Nitric Oxide in Premixed Hydrocarbon Flames, 13^{th} Symposium International of Combustion (1971) 373–379.

[25] C. Schwerdt. Modeling NO_X-Formation in Combustion Processes. MSc Thesis. Department of Automatic Control. Lund University. Sweden.
[26] F. Chmela, M. Engelmayer, G. Pirker and A. Wimmer, Prediction of Turbulence Controlled Combustion in diesel Engines, THIESEL 2004 Conference on Thermo-and Fluid Dynamic Processes in diesel Engines Valencia (2004).
[27] A. Uludogan, D.E. Forester and R.D. Reitz, Modelling the Effect of Engine Speed on the Combustion process and Emissions from diesel Engines, SAE Paper 962056 (1996).
[28] J. B. Heywood, Internal Combustion Engine Fundamentals, McGraw-Hill, New York, 1988.
[29] M.F.J. Brunt, H. Rai and A.L. Emtage, Calculation of Heat Release Energy from Engine Cylinder Pressure Data, SAE Paper 981052 (1998). Appl. Therm. Eng. 26 (2006) 226–236.
[30] F. Payri, S. Molina, J. Martín, O. Armas Influence of measurement errors and estimated parameters on combustion diagnosis. Appl. Therm. Eng. 26 (2006) 226–236.
[31] G. Woschni. A universally applicable equation for the instantaneous heat transfer coefficient in the internal combustion engine. SAE paper 670931 (1967).
[32] G. Woschni. Die Berechnung der Wandverluste und der thermischen Belastung der Bauteile von dieselmotoren. MTZ 31/12 (1970) 491-499.
[33] M. Lapuerta, O. Armas, J.J. Hernández. Diagnosis of DI diesel combustion from in-cylinder pressure signal by estimation of mean thermodynamic properties of the gas, Appl. Therm. Eng. 19 (1999) 513-529.
[34] P.K. Senecal, J. Xin and R.D. Reitz, Prediction of Residual Gas Fraction in IC Engines, SAE Paper 962052 (1996).
[35] F. Payri, M. Lapuerta, P. Cazaux, Insight into combustion process of a diesel engine with exhaust gas recirculation, SIA paper 9506A13 (1995).
[36] J.E. Dec, A Conceptual Model of DI diesel Combustion Based on Laser-sheet Imaging, SAE Paper 970873 (1997).
[37] E. Chaize, D.E. Webster, B. Krutzsch, G. Wennninger, M. Weibel, Sh. Hodjati, C. Petit, V. Pitchon, A. Kiennemann, R. Loenders, O. Monticelli, P.A. Jacobs, J.A. Martens and B. Kasemo, Reduction of NO_X in Lean Exhaust by Selective NO_X-Recirculation (SNR-Technique) Part II: NO_X Storage Materials, SAE Paper 982593 (1998).
[38] B. Krutzsch, G. Wenninger, M.Weibel, P.Stapf, A.Funk, D.E. Webster, E.Chaize, B. Kasemo, J.A. Martens, A Kiennemann, Reduction of NO_X in Lean Exhaustby Selective NO_X-Recirculation (SNR Technique)- part I: System and Decomposition Process, SAE Paper 982592 (1998).
[39] R. Vellaisamy, N. N Clark, G.J. Thompson, R.J. Atkinson, C.A. Tissera, M.M. Swartz, Assessment of NO_X Destructions in Diesel Engines by Injecting NO in the Intake Manifold, SAE Paper 2005-01-0370 (2005).
[40] F. Payri, J.Arregle, J.J López and E. Mocholí, Diesel NO_X Modeling with a Reduction Mechanism for the Initial NO_X Coming from EGR or Re-entrained Burned Gases, SAE Paper 2008-01-1188 (2008).

List of figures

Appendix A. NO_X reduction mechanism calculation

Appendix A.1. Reduction of the NO_X coming from the EGR

If it is assumed that the NO_X mass fraction at the exhaust ($Y_{NO_X,exh}$) remains invariable between exhaust and EGR, the NO_X mass re-entrained is:

$$m_{EGR} \cdot Y_{NO_X,exh} \tag{A.1}$$

The NO_X mass that takes part in the combustion process is then:

$$m_{EGR} \cdot Y_{NO_X,exh} \cdot F_r \tag{A.2}$$

Assuming a reduction efficiency (ε), the NO_X mass diminution is:

$$m_{EGR} \cdot Y_{NO_X,exh} \cdot F_r \cdot \varepsilon \tag{A.3}$$

where ε=1, considering that the 100% of the re-entrained NO_X is destroyed.

The net NO_X mass per cycle that exits from the cylinder is:

$$\begin{aligned} m_{exh} \cdot Y_{NO_X,exh} &= m_{NO_{Xnet}} + m_{EGR} \cdot Y_{NO_X,exh} \cdot (1 - F_r \cdot \varepsilon) \\ m_{NO_{Xnet}} &= Y_{NO_X,exh} \cdot (m_{exh} - m_{EGR} \cdot (1 - F_r \cdot \varepsilon)) \\ &= Y_{NO_X,exh} \cdot (m_a + m_f + m_{EGR} - m_{EGR} \cdot (1 - F_r \cdot \varepsilon)) \\ &= Y_{NO_X,exh} \cdot (m_a + m_f + m_{EGR} \cdot F_r \cdot \varepsilon) \end{aligned} \tag{A.4}$$

where, $m_{NO_{Xnet}}$ is the net NO_X produced in the current combustion and m_{exh} is the gas mass per cycle that exits from the cylinder.

Then the following expression can be obtained:

$$Y_{NO_X,exh} = \frac{m_{NO_{Xnet}}}{m_a + m_f + m_{EGR} \cdot F_r \cdot \varepsilon} \tag{A.5}$$

Appendix A.2. Reduction of the NO_X produced during the combustion process

Thanks to the NO_X reduction mechanism, a part of the NO_X mass produced at the current combustion ($m_{NO_{Xcomb}}$) will be re-entrained, and hence the net NO_X produced at the current cycle ($m_{NO_{Xnet}}$) will be lower. Based on this fact, the following situations can be considered:

1. At the start of combustion (SOC): the efficiency of the NO_X reduction is 0 (none NO_X has been re-entrained).
2. At the end of combustion (EOC): if it is assumed that all the combustion products are homogeneously mixed in the chamber, the efficiency will be F_r.

In order to consider all the combustion evolution it is assumed the intermediate situation: $K_{re} \cdot F_r$, where $K_{re} = 0.5$.

Taking into account the efficiency ε of the NO_X reduction mechanism (in this case related to the NO_X produced and re-entrained), the following expression is obtained:

$$m_{NO_{X\,net}} = m_{NO_{X\,comb}} \cdot (1 - K_{re} \cdot F_r \cdot \varepsilon) \tag{A.6}$$

Therefore, the relationship between $m_{NO_{X\,comb}}$ and $Y_{NO_X,exh}$ is:

$$Y_{NO_X,exh} = \frac{m_{NO_{X\,comb}} \cdot (1 - K_{re} \cdot F_r \cdot \varepsilon)}{m_a + m_f + m_{EGR} \cdot F_r \cdot \varepsilon} \tag{A.7}$$

Table(s)

	Dimension	Units
Bore	85	[mm]
Stroke	96	[mm]
Unitary piston displacement	545.75	$[cm^3]$
Connecting rod length	152	[mm]
Compression ratio	17:1	[-]

Table 1: Engine characteristics.

Speed [rpm]	Model development [Load %]	Model validation [Load %]
780	idle	-
1000	35, 55	70, Full load
1500	30, 45	10, 75
2000	15, 45, 58	25, 65, Full load
2500	35, 45, 58	15, 75
2850	20, 40	55, Full load
3000	15	40, 70, Full load
3500	-	10, 20, 40, 70, Full load
4000	-	15, 40, 70, Full load

Table 2: Operating points used for development and validation of the model.

	Mean absolute error [mg/str]		Mean relative error [%]	
	Training data	Validation data	Training data	Validation data
$K_{1,2,3\ Local\ fitting}$	0.0489	0.2296	14.48	15.83
$K_{1,2,3\ Global\ fitting}$	0.0499	0.3173	17.96	18.39
$K_{3\ Global+corrected}$	0.0421	0.2163	15.12	17.71

Table 3: Model fitting mean errors.

		Combustion diagnostic	
	Fast dQ_b	Complete	Simplified
Calculation time [ms]	4	487	4.5
Relative error [%]	15.6	9.5	10.2

Table 4: Calculation time and accuracy of the model using different methods to calculate dQ_b.

Figure 1

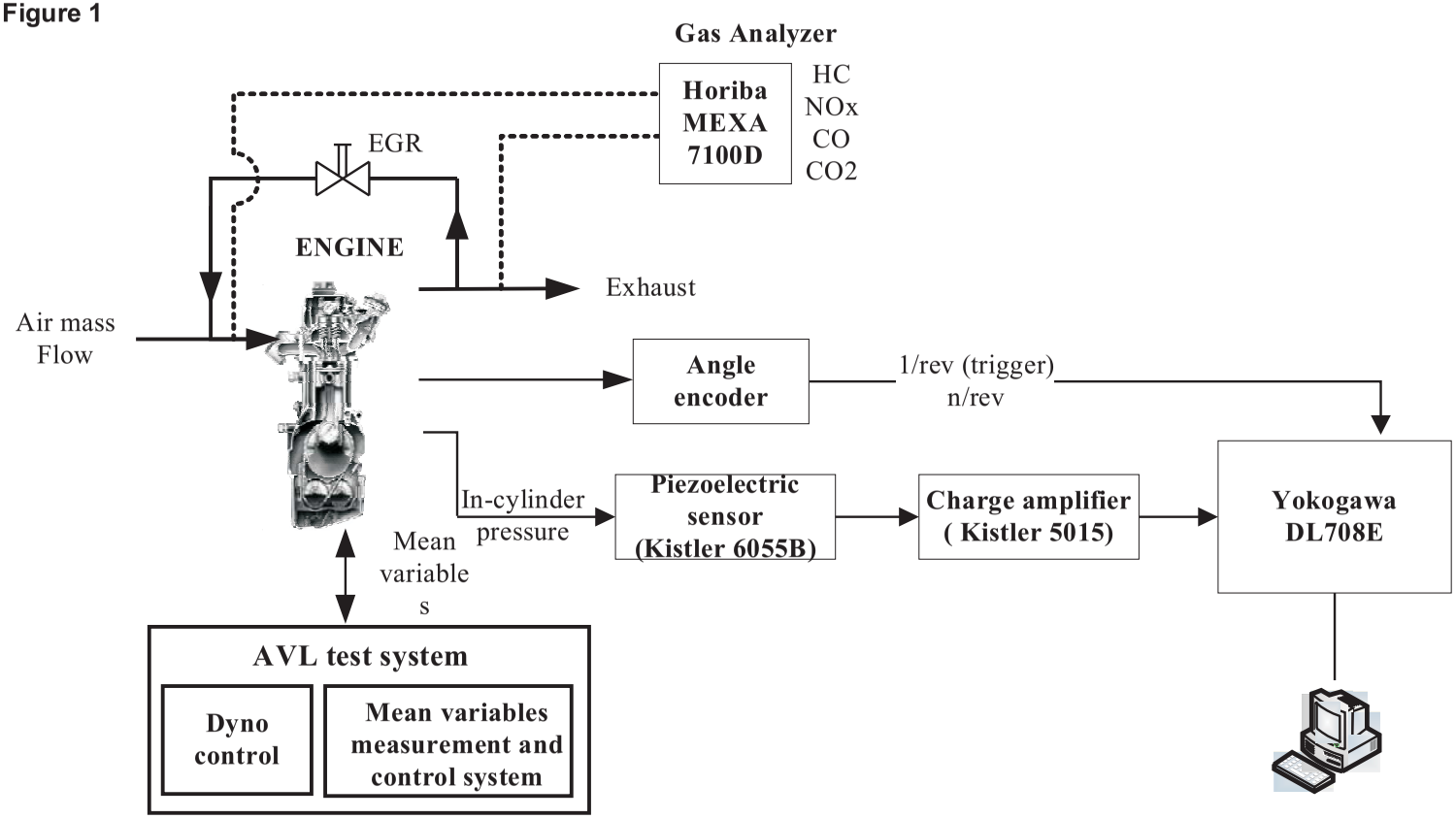
Gas Analyzer
Horiba MEXA 7100D
HC
NOx
CO
CO2
EGR
ENGINE
Exhaust
Air mass Flow
Angle encoder
1/rev (trigger)
n/rev
In-cylinder pressure
Piezoelectric sensor (Kistler 6055B)
Charge amplifier (Kistler 5015)
Yokogawa DL708E
Mean variable s
AVL test system
Dyno control
Mean variables measurement and control system

Figure 2

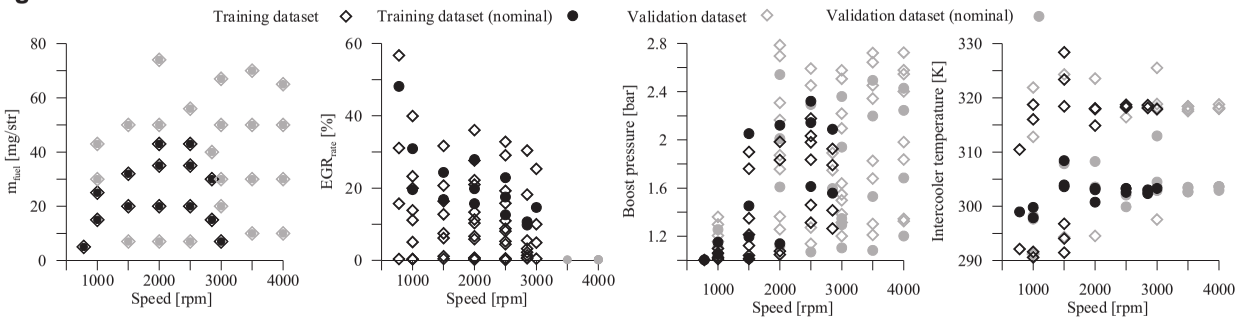
Training dataset
Training dataset (nominal)
Validation dataset
Validation dataset (nominal)
m_{fuel} [mg/str]
EGR_{rat} [%]
Boost pressure [bar]
Intercooler temperature [K]
Speed [rpm]
1000
2000
3000
4000

Figure 3

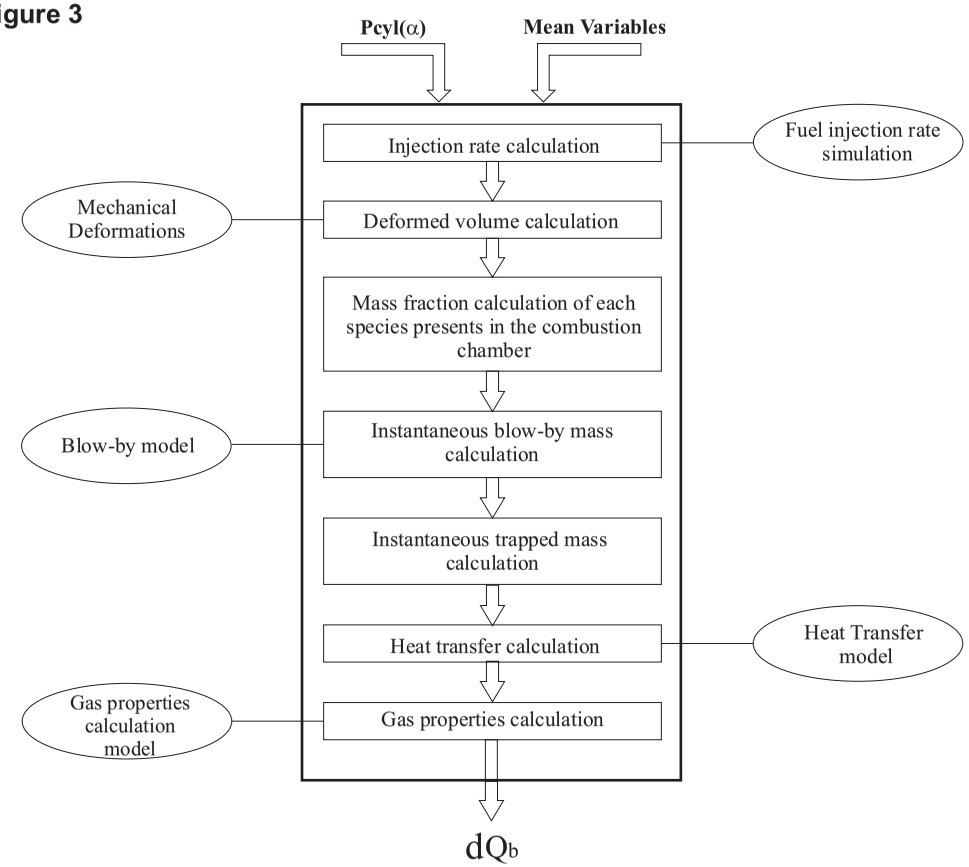
Pcyl(α)
Mean Variables
Injection rate calculation
Fuel injection rate simulation
Mechanical Deformations
Deformed volume calculation
Mass fraction calculation of each species presents in the combustion chamber
Blow-by model
Instantaneous blow-by mass calculation
Instantaneous trapped mass calculation
Heat transfer calculation
Heat Transfer model
Gas properties calculation model
Gas properties calculation
dQb

Figure 4

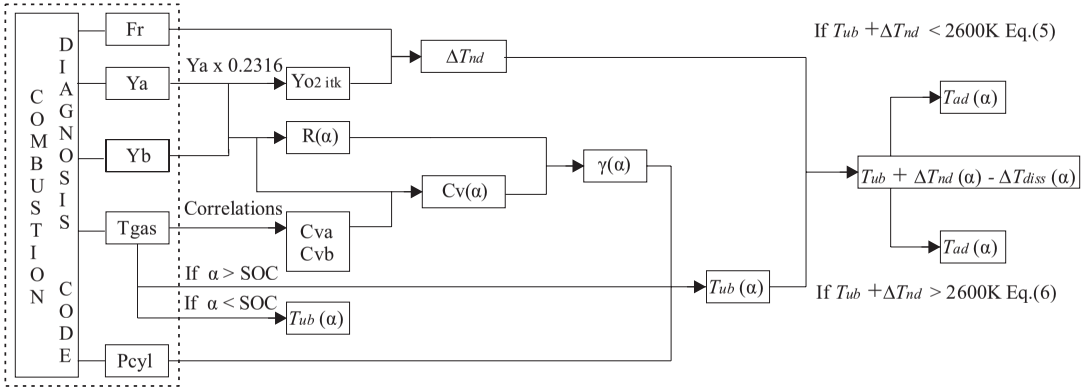
COMBUSTION DIAGNOSIS CODE
Fr
Ya
Yb
Tgas
Pcyl
Ya x 0.2316
Yo2 itk
ΔTnd
R(α)
Cv(α)
γ(α)
Correlations
Cva
Cvb
If α > SOC
If α < SOC
Tub (α)
Tub (α)
If Tub +ΔTnd < 2600K Eq.(5)
Tad (α)
Tub + ΔTnd (α) - ΔTdiss (α)
Tad (α)
If Tub +ΔTnd > 2600K Eq.(6)

Figure 5

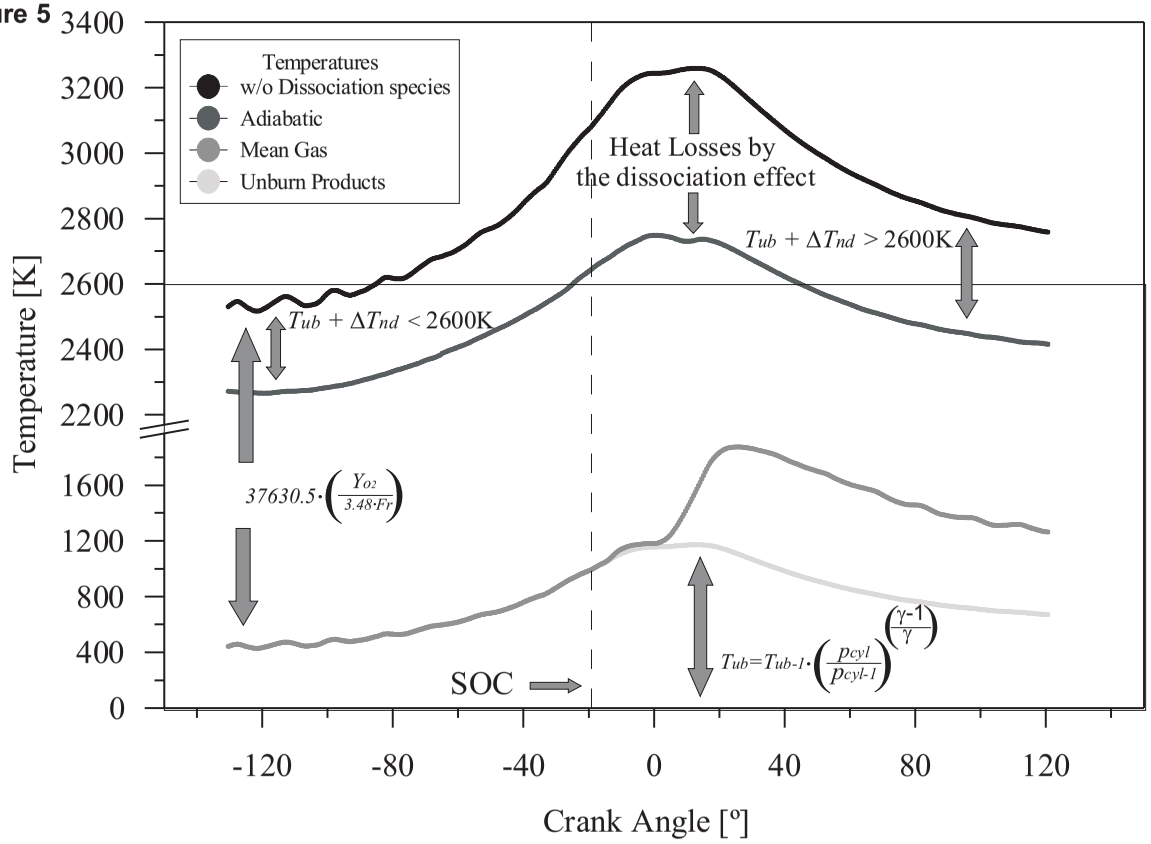
Temperatures
w/o Dissociation species
Adiabatic
Mean Gas
Unburn Products
Heat Losses by
the dissociation effect
Tub + ΔTnd > 2600K
Tub + ΔTnd < 2600K
37630.5·(Yo2 / 3.48·Fr)
Tub=Tub-1·(pcyl / pcyl-1)^((γ-1)/γ)
SOC
Temperature [K]
Crank Angle [º]
3400
3200
3000
2800
2600
2400
2200
1600
1200
800
400
0
-120
-80
-40
0
40
80
120

Figure 6

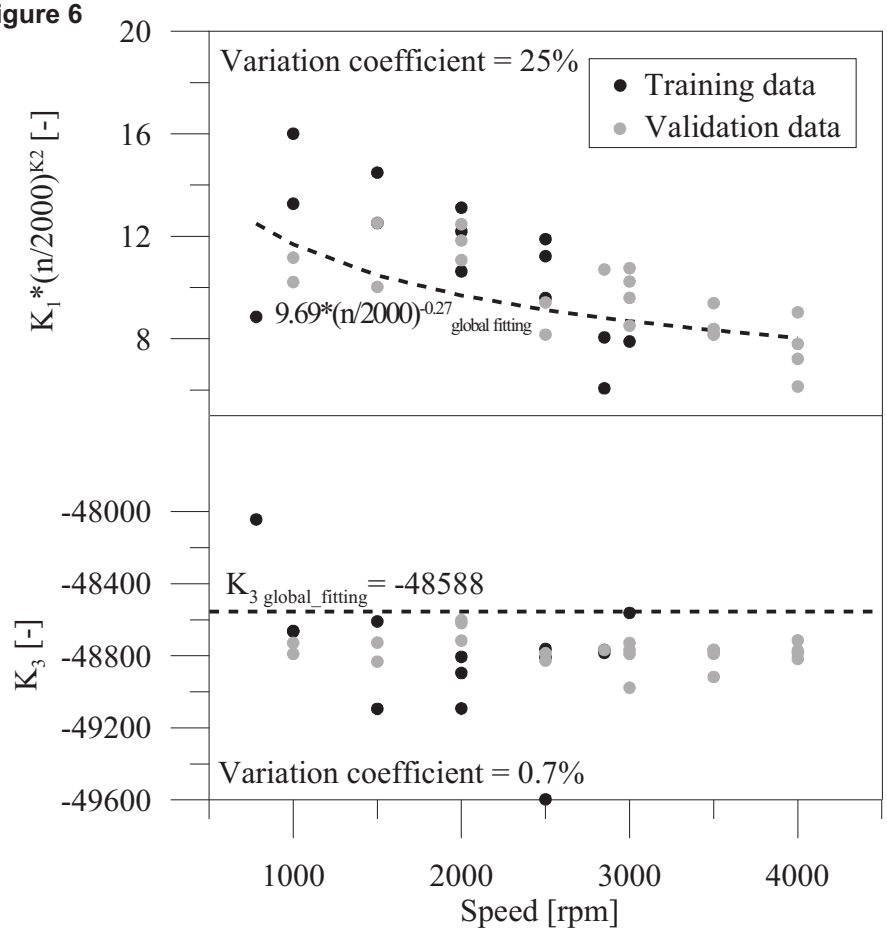
Variation coefficient = 25%
Training data
Validation data
$K_1*(n/2000)^{K2}$ [-]
20
16
12
8
$9.69*(n/2000)^{-0.27}$ global fitting
-48000
-48400
-48800
-49200
-49600
K_3 [-]
$K_{3\ global\_fitting}$ = -48588
Variation coefficient = 0.7%
1000
2000
3000
4000
Speed [rpm]

Figure 7

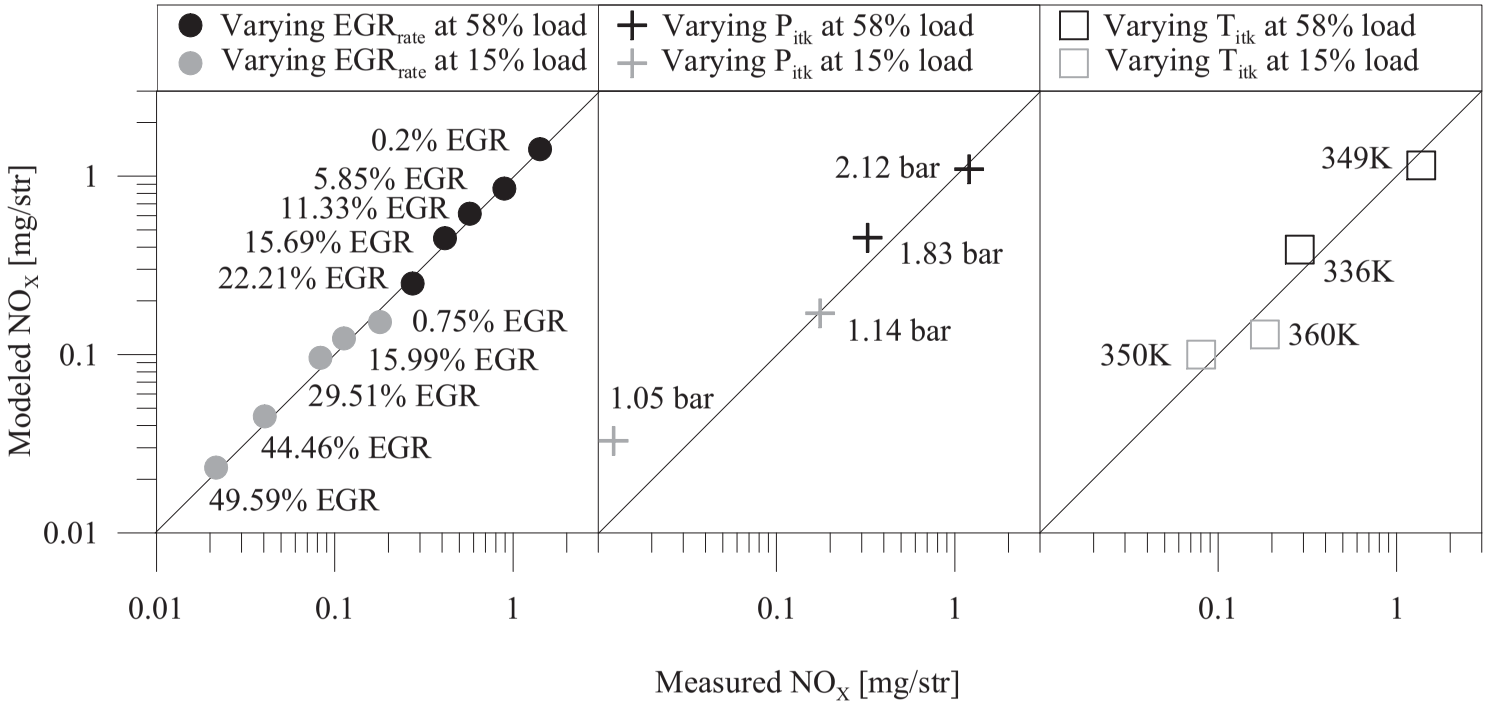
Varying EGR$_{rate}$ at 58% load
Varying EGR$_{rate}$ at 15% load
Varying P$_{itk}$ at 58% load
Varying P$_{itk}$ at 15% load
Varying T$_{itk}$ at 58% load
Varying T$_{itk}$ at 15% load
0.2% EGR
5.85% EGR
11.33% EGR
15.69% EGR
22.21% EGR
0.75% EGR
15.99% EGR
29.51% EGR
44.46% EGR
49.59% EGR
2.12 bar
1.83 bar
1.14 bar
1.05 bar
349K
336K
360K
350K
Modeled NO$_X$ [mg/str]
Measured NO$_X$ [mg/str]
0.01
0.1
1

Figure 8

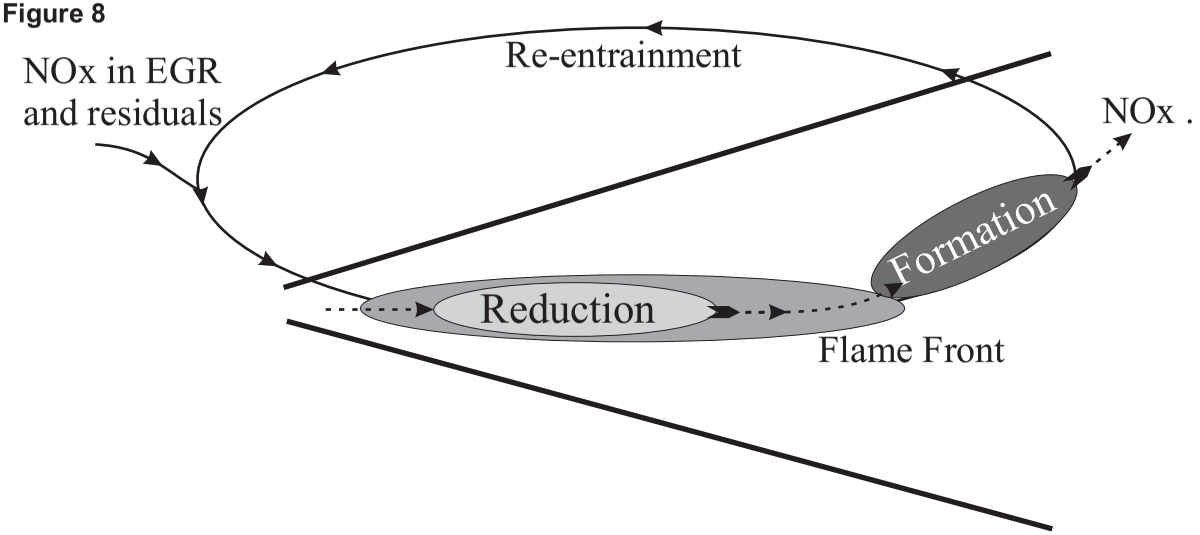
NOx in EGR
and residuals
Re-entrainment
NOx .
Formation
Reduction
Flame Front

Figure 9

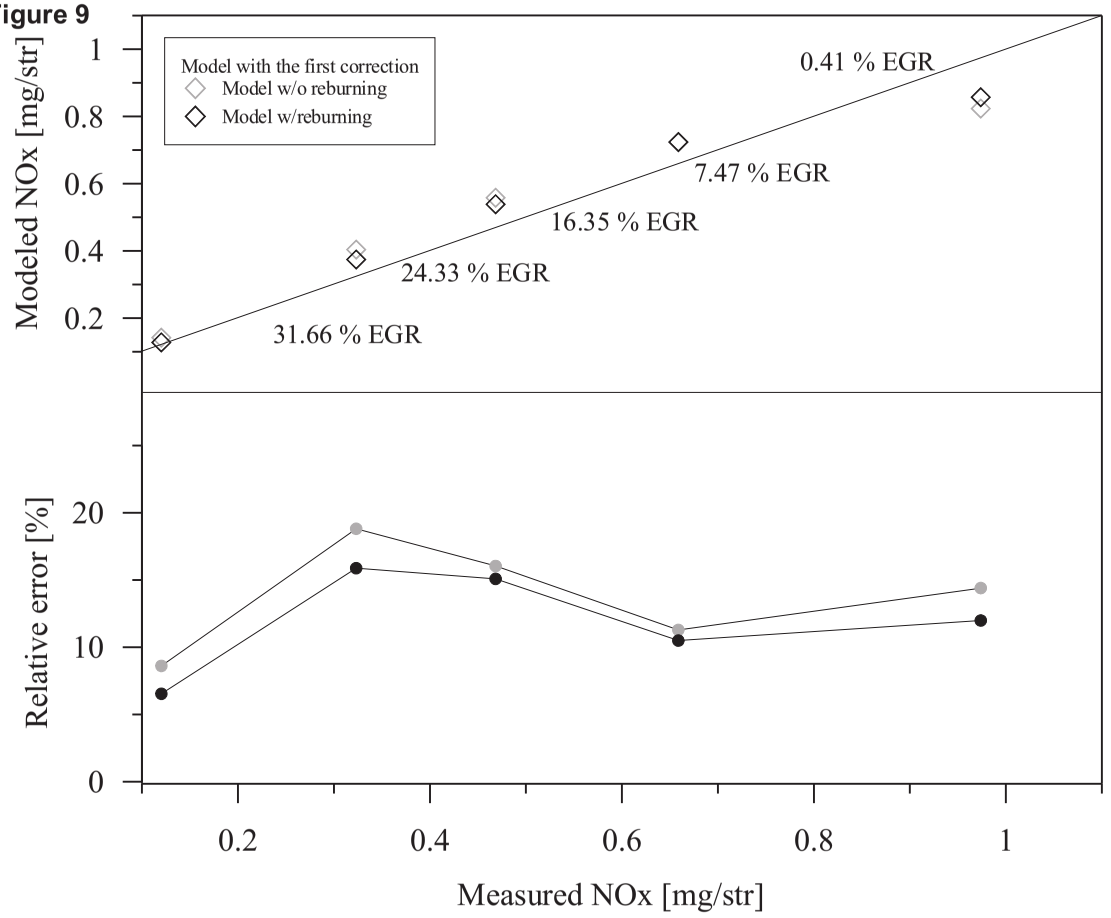
Model with the first correction
Model w/o reburning
Model w/reburning
Modeled NOx [mg/str]
1
0.8
0.6
0.4
0.2
0.41 % EGR
7.47 % EGR
16.35 % EGR
24.33 % EGR
31.66 % EGR
Relative error [%]
20
10
0
0.2
0.4
0.6
0.8
1
Measured NOx [mg/str]

Figure 10

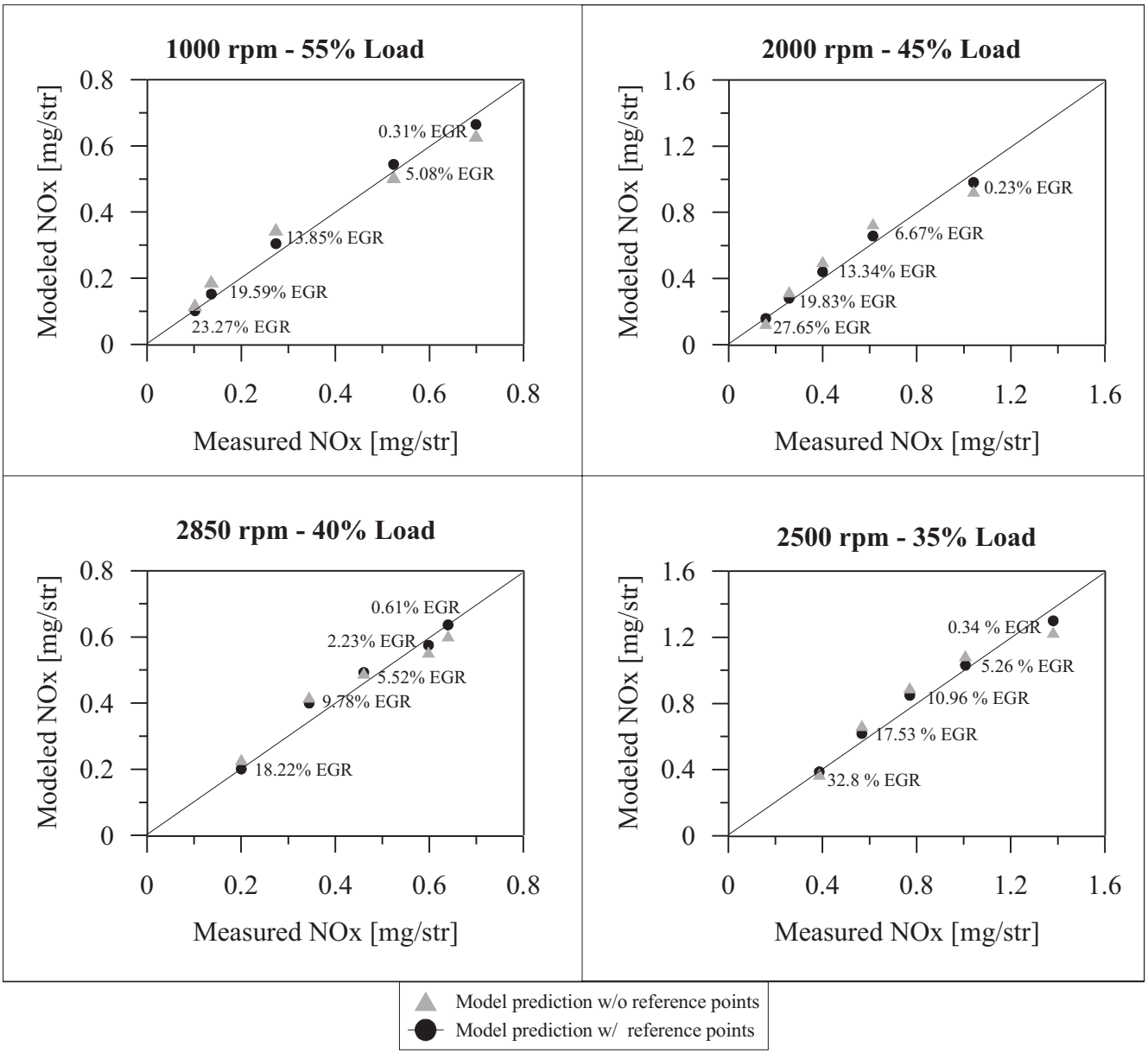
1000 rpm - 55% Load
Modeled NOx [mg/str]
Measured NOx [mg/str]
0.31% EGR
5.08% EGR
13.85% EGR
19.59% EGR
23.27% EGR
2000 rpm - 45% Load
0.23% EGR
6.67% EGR
13.34% EGR
19.83% EGR
27.65% EGR
2850 rpm - 40% Load
0.61% EGR
2.23% EGR
5.52% EGR
9.78% EGR
18.22% EGR
2500 rpm - 35% Load
0.34 % EGR
5.26 % EGR
10.96 % EGR
17.53 % EGR
32.8 % EGR
Model prediction w/o reference points
Model prediction w/ reference points

Figure 11

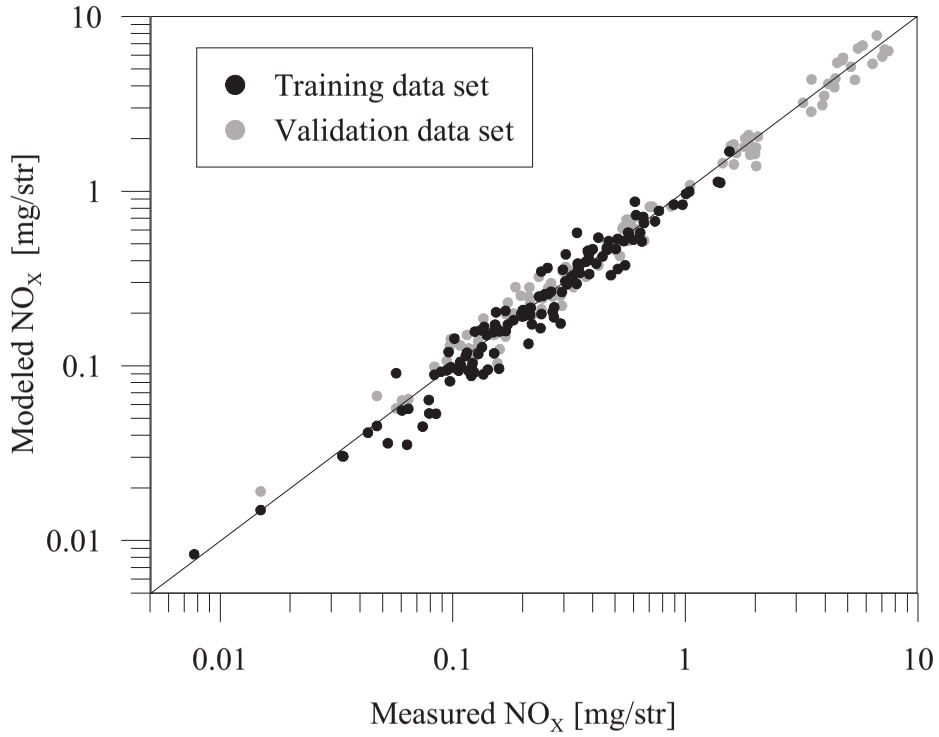
Training data set
Validation data set
Modeled NO_X [mg/str]
Measured NO_X [mg/str]
10
1
0.1
0.01
0.01
0.1
1
10